Hydrol. Earth Syst. Sci. Discuss., 10, 7045–7089, 2013
www.hydrol-earth-syst-sci-discuss.net/10/7045/2013/
doi:10.5194/hessd-10-7045-2013

Hydrology and Earth System Sciences
Open Access
Discussions

A paradigm shift in predicting stormflow responses in an active tectonic region through a similarity analysis of pressure propagation in a hydraulic continuum

Makoto Tani

Laboratory of Forest Hydrology, Graduate School of Agriculture, Kyoto University, Kitashirakawa, Sakyo, Kyoto, 606-8502, Japan

Received: 19 May 2013 – Accepted: 21 May 2013 – Published: 3 June 2013

Correspondence to: Makoto Tani (tani@kais.kyoto-u.ac.jp)

Published by Copernicus Publications on behalf of the European Geosciences Union.

Abstract

Soil layers on hillslopes acts as systems in quasi-steady states generating rainfall-stormflow responses that are controlled by pressure propagation in a hydraulic continuum established when the rainfall volume is sufficiently large. A similarity analysis for quantifying the sensitivity of the stormflow response and recession limb to topographic and soil properties in a sloping permeable domain showed that the deviation of stormflow responses in the hydraulic continuum decreases due to the macropore effect. The rapid responses seem to be naturally derived from the evolution of the soil layer with the assistance of the vegetation-root system and effective drainage systems in zero-order catchments in active tectonic regions with heavy storms. To predict stormflow responses using distributed runoff models, a paradigm shift to consider this evolution process is needed because the simple stormflow responses and complex and heterogeneous catchment properties are poorly related, but may be mainly determined by soil evolution processes.

1 Introduction

The prediction of runoff response to rainfall is a basic hydrological aim. Since the successful applications of the tank model to many rivers (Sugawara and Katsuyama, 1957; Sugawara, 1995), numerous models have been developed for this purpose. However, it is still difficult to estimate hydrographs in response to hyetographs without a parameter calibration using previous observational data (Sivapalan et al., 2003). There are many reasons for this, but the most essential one is the difficulty in detecting the main properties of a catchment that control its runoff responses (Betson and Ardis Jr., 1978). Most physically-based distributed runoff models assume that the surface topography is the controlling factor (e.g., Beven and Kirkby, 1979; O'Loughlin, 1986). However, some hillslope observations, especially in active tectonic regions, do not indicate the dominant effects of topography. This incompatible observational result

HESSD
10, 7045–7089, 2013

is attributable to the dominant function of underground pathways, including weathered bedrock (Montgomery and Dietrich, 2002; Kosugi et al., 2006; Gabrielli et al., 2012). Kosugi et al. (2011) demonstrated that a localized bedrock aquifer distribution not following the catchment topography produced a unique triple-peak hydrograph response in a headwater catchment. Katsuyama et al. (2010) compared five small subcatchments and showed that the mean residence time of each was explained not by the topography but by the deep percolation ratio estimated from the annual water balance. Sugawara (1979), in his textbook on runoff analysis, referred to the following off-target behavior: a miserable man searches for his missing key only within an obvious circle illuminated by a streetlight because of the outside darkness, even though his key could have been lost anywhere. This analogy may apply to the developers of distributed runoff models, who have built their models based on the surface topography. However, sensitive catchment properties are also embedded underground, outside the obvious area. Difficulties in PUB (prediction of ungauged basins) (Sivapalan et al., 2003) are closely related to the problem of not considering underground structures.

For stormflow responses, many distributed runoff models still use the surface flow for their pathways, although observations of hillslope hydrology have not accepted this concept (McDonnell, 2003). Early in the field of hydrology, stormflow was considered to be the infiltration-excess overland flow (Horton, 1933). This concept produced simple kinematic-wave routine models (Sueishi, 1955; Iwagaki, 1955). Although the role of subsurface flow was also noted, because of the high infiltration capacity of forest soils (Hewlett and Hibbert, 1968), the saturation-excess overland flow was considered as a source of stormflow responses even into the 1960s (Dunne and Black, 1970; Freeze, 1972). Because of the low velocity of subsurface flow, such stormflow responses could not be separated from the total runoff discharge, but was represented by the high-speed water movement of overland flow. Many distributed runoff models still in use today are based on this concept of saturation-excess overland flow (Ishihara and Takasao, 1964; Beven and Kirkby, 1979). By tracer investigations (Pinder and Jones, 1969; Sklash and Farvolden, 1979), however, the important contribution of pre-event

HESSD
10, 7045–7089, 2013

soil water to stormflow was detected, and many well-designed observations were conducted to explain the production of stormflow by soil water movement (Mosley et al., 1979; Pearce et al., 1986; McDonnell, 1990). We now understand that both the quick flow within preferential pathways and quick pressure propagation originating from the slow water movement within a soil matrix play important roles in the stormflow generation processes (Anderson et al., 1997; Tani, 1997) as also reviewed in Sect. 2 of this paper. Although quantifying the source of water in each storm event requires further study (Gomi et al., 2010), it is irrefutable that the water movement within a soil layer can produce stormflow.

Nevertheless, a new question has emerged: previous studies could not demonstrate why water movement within a soil layer resulted in the production of stormflow. A hydrograph generally has rising and falling inflection points. Although the latter are usually vague, the recession timescales beforehand and afterwards are quite different. In an active tectonic region like Japan, the half-life of a recession limb before the inflection point usually ranges from several hours to one day, although that after the point may be larger than several days (Okamoto, 1978). Double or triple peaks are sometimes generated in small catchments, as mentioned before (Onda, 2001; Kosugi et al., 2011), but the responses of river flow to rainfall commonly contain a quick component of stormflow with a short half-life distinguished from the entire hydrograph. Although this question may be unique and not generally addressed, it is believed to provide important information on stormflow mechanisms and modelling.

Two considerations are addressed in this paper. First, the stormflow responses observed in small catchments consisting of steep hillslopes are reviewed in Sect. 2. We conclude that when the total rainfall is large enough, the mechanism for stormflow production can be attributed to pressure propagation in a hydraulic domain. In Sects. 3 and 4, a similarity analysis on the saturated and unsaturated flow components within a sloping permeable domain are performed to quantify the pressure propagation. The effects of the topographic and soil properties and macropores on the stormflow response and recession limb are quantitatively evaluated using this analysis. On the basis of our

HESSD
10, 7045–7089, 2013

results, the discussion in Sect. 5 focuses on why quick stormflow responses are generally produced from zero-order catchments in an active tectonic region. The findings will contribute to a new strategy for evaluating the effects of catchment properties on runoff responses.

2 Review of stormflow response observations

2.1 Allocation of rainfall to stormflow

The relationship of stormflow volume per unit catchment area to the total rainfall volume in each storm event has been frequently illustrated as a means to understand the storm runoff characteristics in a catchment (Soil Conservation Service, 1972; Okamoto, 1978). When the rainfall is small, the stormflow is low because most of the rainwater is stored in the soil layer by absorption within small pores with a low matric potential. There, water can be extracted only by evapotranspiration with a supply of latent heat. It cannot be drained by gravity. For stormflow volumes that increase with rainfall, a threshold value was detected in some catchments, suggesting the saturation of small pores (Tani, 1997; Tromp-van Meerveld and McDonnell, 2006). The loss of the stormflow volume is also derived from percolation into deep layers, such as weathered bedrock (Kosugi et al., 2006). This quantitatively depends on the underground structure represented by the surface geology. The loss is large for mountainous catchments with granite, but small for those with sedimentary rock, causing a clear difference in the flow duration curves between those catchment types (Shimizu, 1980). Figure 1 shows an example for a small catchment in Japan with each type of geology: Kiryu (Katsuyama et al., 2008) and KT in the Tatsunokuchi-yama Experimental Forest (TEF), Okayama, Japan (Tani and Abe, 1987). After the cumulative rainfall exceeds the threshold volume in a large-scale storm, almost all the rainwater tends to be allocated to the stormflow, at least in catchments with sedimentary rock (Tani and Abe, 1987). Therefore, we can imagine that the entire catchment area eventually contributes to the stormflow

HESSD
10, 7045–7089, 2013

production, even though some rainwater may still be allocated to deep percolation in catchments with geologies such as granite. Next, we examine two observation results for such wet conditions during storms.

2.2 Stormflow responses as pressure propagation under wet conditions

A valuable study of sprinkling experiments was conducted in the Oregon Coast Range, USA, to understand the stormflow mechanism under the ground (Anderson et al., 1997; Montgomery et al., 1997; Ebel et al., 2007). The site labelled CB1 was a steep zero-order catchment (860 m^2 and 43°) on Eocene volcaniclastic sandstone bedrock. Rainfall of a relatively weak intensity (average of 1.65 $mm\,h^{-1}$) was supplied for a long duration (7 days), and all the water infiltrated into the soil. Two weirs (upper and lower) measured flow rates from both colluvium and fractured bedrock in the catchment, where the flow through the upper weir was separated from that through the lower weir, which was located 15 m downstream. As shown in Fig. 2, the flow rates measured at the upper and lower weirs were roughly constant, equal to about one third of the supplied rainwater intensity. Both the flow rates had a daily oscillation due to evapotranspiration and wind-induced variations in the rainfall intensity. The rainfall intensity with a large spatial distribution was manually measured twice daily and the flow rate at each weir was measured by hand. Thus temporal changes could not be recorded in detail (Ebel et al., 2007), and the results illustrated in Fig. 2 can be only used for a rough comparison because of the time lags. However, the results indicated that during the 4-day period when the flow was nearly steady, the rainfall of 1.65 $mm\,h^{-1}$ was allocated to the averaged total flow rate of 1.1 $mm\,h^{-1}$. The deep infiltration constituted a leakage of 0.5 $mm\,h^{-1}$, with the rest going to evapotranspiration (Anderson et al., 1997).

Figure 2 clearly shows the two types of loss mentioned above: absorption within small pores with low matric potential and percolation into deep layers. The former loss type was detected from the small flow rate in the early stage, and the latter was estimated as the leakage of 0.5 $mm\,h^{-1}$ that remained even during the later stage in a nearly steady state. The flow rate through each of the weirs roughly responded with a

HESSD
10, 7045–7089, 2013

delay in the oscillation of rainfall intensity during the nearly steady state, regardless of the limitations of the hand measurements. For the flow response to rainfall, Anderson et al. (1997) found the following processes through two kinds of tracer experiments. A high speed subsurface flow from the fractured bedrock to the outlet through the colluvium was detected by bromide point injections into the saturated materials. Another experiment using sprinkler water labelled by deuterium showed a plug flow without preferential flow for the vertical unsaturated water movement. These tracer experiments strongly suggested that a combination of a vertical plug flow in the unsaturated zone and a high-speed preferential downslope flow in the saturated zone may produce quick flow responses to rainfall. In these processes, storage fluctuations may have caused the small delay of the flow discharge both in the vertical unsaturated flow and the saturated downslope flow in response to the rainfall oscillation in a nearly steady state. The former flow is described by Darcy's Law, where the volumetric water content in the unsaturated zone increases and decreases in response to fluctuations in the rainfall rate, due to the vertical flow rate being a monotonically increasing function of water content (Rubin and Steinhardt, 1963). The latter originated from the water table as the downslope flow rose and fell in response. These processes should generally follow the hydraulics of water pressure propagation, even though water moves at quite different speeds through unsaturated soil and a pipe channel.

Similar pressure propagation was estimated from two small forested catchments, KT (17.3 ha) and MN (22.6 ha), in TEF (Tani, 1997). The soil was a clay loam derived from the sedimentary rock. Although the soil was generally deep, the two catchments were both characterized by high stormflow volumes, where most of the rainfall was allocated to the stormflow under wet conditions when the rainfall volume exceeded the threshold of cumulated rainfall. The value of the latter depended on the antecedent catchment dryness before each storm event. For quick flow responses, the vertical water movement was estimated not as a preferential flow but as the unsaturated flow through the soil matrix, because the matric potential measured in the soil layer on a steep planar hillslope (500 m^2 and 35°) had a clear positive relationship to the given rainfall

HESSD
10, 7045–7089, 2013

intensity, as expected from Darcy's Law (Rubin and Steinhardt, 1963). In addition, the groundwater level at 15 m depth in a steep zero-order catchment increases quickly in response to rainfall, similar to the stormflow rate during wet conditions in an upper soil layer, although the level does not respond during dry soil conditions (Hosoda, 2008). Quick downslope water movement was not explicitly detected, unlike in CB1, but a quick stormflow response with volume comparable to that of rainfall frequently occurred without overland flow in these catchments. This result suggested that these stormflow characteristics may be caused only by the mechanism of water pressure propagation, as in the CB1 catchment.

2.3 Tank approach to quantifying the stormflow response

A tank with a drainage hole is a typical component of many storage-type runoff models such as the tank model (Sugawara, 1995), HYCYMODEL (Fukushima and Suzuki, 1988), and TOPMODEL (Beven and Kirkby, 1979). These models commonly contain an algorithm for the rainwater allocation to tanks producing stormflow and baseflow. However, in our two catchments KT and MN in TEF, almost all the rainfall was allocated to the stormflow under wet conditions as already mentioned in Sect. 2.1 with Fig. 1. For this case, we can describe a model of the rainfall-stormflow response without an algorithm of the rainfall allocation, the so-called effective rainfall separation, as

$$\frac{dV}{dt} = r - f \tag{1}$$

$$V = kf^p \tag{2}$$

where V is the storage, r is the rainfall intensity, f is the flow rate (all per unit catchment area), and k and p are parameters. Equation (1) represents the water balance as a physical law, but the storage and flow relationship in Eq. (2) is empirical.

Figure 3 shows the simulated stormflow responses in the KT and MN catchments to a typhoon storm in September 1976, with a total rainfall of 375 mm. Ten-minute

HESSD
10, 7045–7089, 2013

rainfall and runoff data were used here, and the rainfall was directly inputted to the tank. The baseflow rate before the storm event was very small (0.0053 mm h^{-1} for KT and 0.0067 mm h^{-1} for MN); thus we neglected the effect of the baseflow increase on the hydrograph during the event. The later stage of the entire event after the catchments reached a wet condition is plotted in Fig. 3. The optimized value of p for both catchments was 0.3, and the values of k for KT and MN were 25 and 40, respectively. Extremely close agreement was obtained for each of the catchments, and the lower peaks and gentler recession limbs for MN vs. KT were accurately simulated by the difference in k between them. This probably reflects thicker soil layers with gentler slopes in MN than KT, considering that there was a slightly larger annual evapotranspiration for MN than KT, as estimated from the 69 yr annual water balance there (Tani and Hosoda, 2012).

For CB1, it was difficult to evaluate the simulation results in terms of runoff responses by a tank with a drainage hole during the nearly steady state, due to the manual measurements of rainfall intensity and runoff rate. However, the recession stage of runoff records was simulated for each of the upper and lower weirs (Fig. 2). An optimized value of p of 0.3 was also used here, and the optimized values of k were 11 and 20 for the upper and lower weirs, respectively. The values of k were slightly lower than those of TEF, but the hydrographs for these catchments were commonly characterized by quick recession limbs separated from those of the baseflow. They were simulated by a simple function with a small range of half-life (roughly from several hours to one day), despite the large differences in catchment properties between them.

2.4 Insensitivity of the stormflow response to storm magnitude

For TEF and CB1, we have so far looked at stormflow responses during conditions in which the entire catchment is wet. Next, we investigate the responses to small volumes before the wet conditions during the storm in TEF. Figure 4 shows hydrographs including the early dry stage in KT. The same calculated hydrograph as that in Fig. 3 and a recession flow calculated for a long no-rain period using the same parameter values

HESSD
10, 7045–7089, 2013

were plotted on a single logarithmic chart, where the recession flow calculated with $p = 1$ is plotted as a straight line. The gradient of the calculated recession hydrograph (broken line) became gentler with time owing to the non-linear function with $p = 0.3$ in Eq. (2). Nevertheless, each of the small observed hydrographs in the early stage had a similar recession gradient to that in the later stage, suggesting that the recession gradient was rather constant, regardless of the magnitude of the storm hydrograph. This might be explained by the so-called variable source area concept (Hewlett and Nutter, 1970), but two mechanisms may be possible: one may be estimated from a downslope process, where a small stormflow would be produced from a short limited pathway of the hillslope. An application of a kinematic wave runoff model to the typhoon storm in September 1976 in TEF, shown in Figs. 3 and 4 (Tani and Abe, 1987), suggested that a pathway extension was one possible mechanism, although no other evidence of this was observed. Another mechanism could be a combination of the vertical unsaturated flow and a rapid downslope flow through preferential pathways such as natural pipes, because the time delay in the hydrograph recession is mainly attributed to vertical pressure propagation. This idea originated from research in CB1 (Montgomery and Dietrich, 2002). These mechanisms can both be involved in situ, and separating them may be difficult. However, both mechanisms are able to produce a constant recession gradient throughout a large range of stormflow magnitudes.

2.5 Similarity of stormflow responses among catchments

The accurate simulation results for TEF and CB1 shown above suggest that stormflow responses could be entirely represented by a pressure propagation simulated by a tank with a drainage hole, even though plural flow mechanisms with different speeds were involved. This simple characteristic for stormflow responses was widely detected in runoff model applications. Practical stormflow analyses for flood management purposes in headwater catchments in Japan have provided examples of successful applications (Kimura, 1961; Sugiyama et al., 1997). Another example is an application of HYCYMODEL to seven small mountainous catchments (Tani et al., 2012). This model

HESSD
10, 7045–7089, 2013

had a tank with a drainage hole as part of the stormflow response. This application demonstrated that stormflow responses in catchments with different land-use histories were similar, except for a catchment covered with bare land, where overland flow was dominant. These observational and model studies demonstrate the applicability of the storage-flow relationship in Eq. (2) to stormflow. The range of recession limbs in each catchment may be rather small in contrast to the large variations in topographic and soil properties.

3 Sensitivity analysis of runoff buffering potential

3.1 Hydraulic continuum characterized by a quasi-steady-state system

The observation results presented in the previous section suggest that the stormflow responses were created through pressure propagation and could be simulated by a tank with a drainage hole after the soil became sufficiently wet due to a large supply of rainfall. Such a tank can be generally regarded as a "quasi-steady-state system", in which a dynamic equilibrium of storage is established when the inflow and outflow rates are the same and the outflow gradually decreases, keeping the same functional relationship of storage to outflow rate as that during the dynamic equilibrium after the inflow rate stops (Meadows, 2008). This character of quasi-steady state systems can be hydraulically derived from pressure propagation under gravity. This is typically described as Darcy's law both in saturated and unsaturated zones in a permeable domain. However, the domain consists of both a soil matrix and preferential paths such as macropores or natural pipes with fast water movement demonstrated by tracer experiments (Mosley, 1979; Anderson et al., 1997). Such simple pressure propagation in a quasi-steady state is important for understanding the essential characteristics of stormflow responses. We refer to this system as a "hydraulic continuum" for the production of stormflow.

HESSD
10, 7045–7089, 2013

The hydraulic continuum for stormflow production was qualitatively characterized by a quasi-steady state and conceptualized by a tank with a drainage hole. Next the quantitative properties of the continuum are analysed. The water balance in Eq. (1) is transformed to

$$\frac{\mathrm{d}f}{\mathrm{d}t} = \frac{r - f}{\mathrm{d}V/\mathrm{d}f} \tag{3}$$

This equation states that when $f = r$, f is constant, but when $f > r$, f increases and when $f < r$, f decreases. In addition, the increase/decrease rate of f is controlled by $\mathrm{d}V/\mathrm{d}f$. Therefore, if the system is in a quasi-steady state, the increase/decrease speed of the flow rate is simply controlled by the differential coefficient of storage with respect to the flow rate in a steady state in Eq. (3).

The left panel of Fig. 5 is a schematic example showing the response of the flow rate to a fluctuation in the rainfall rate, the average of which is $1\,\mathrm{mm\,h^{-1}}$. The relationships between storage and flow rate are represented by Eq. (2) as illustrated in the right panel of Fig. 5. We used a common p value of 0.3 and three k values of 10, 25, and 40 in Eq. (2) in reference to the results from CB1 and TEF. The figure clearly shows the dependency of the increase/decrease speed of f on $\mathrm{d}V/\mathrm{d}f$, not only during dynamic equilibrium but also in the recession stage.

3.2 Link between the hydraulic continuum and runoff buffering potential

Equation (3) demonstrates the importance of the storage and flow-rate relationship in evaluating the speed of the flow rate quantitatively in response to the rainfall fluctuation in a hydraulic continuum. Tani (2008) has already proposed this relationship for a sloping permeable domain and defined the runoff buffering potential (RBP) as the difference between the water storage volumes integrated over the domain in response to two steady-state runoff rates (f_a and f_b) given to the system. Hence

HESSD
10, 7045–7089, 2013

$$\mathrm{RBP} = \int_{f_a}^{f_b} \frac{\mathrm{d}V}{\mathrm{d}f}\mathrm{d}f = V(f_a) - V(f_b) \tag{4}$$

Here, this integral equation is converted into a differential form as

$$\mathrm{RBPI}\,\big|_{f_m} \equiv \frac{\mathrm{d}V}{\mathrm{d}f}\,\big|_{f_m} \tag{5}$$

where RBPI is the index of the RBP, and f_m is the averaged flow rate around which f fluctuates. In the recession stage from a storm event, substituting Eq. (5) into Eq. (3) gives the recession gradient at f_m as

$$\frac{\mathrm{d}f}{\mathrm{d}t}\,\big|_{f_m} = \frac{-f_m}{\mathrm{d}V/\mathrm{d}f\,\big|_{f_m}} = \frac{-f_m}{\mathrm{RBPI}\,\big|_{f_m}} \tag{6}$$

Hence the half-life (T_h) at f_m is described as

$$T_h\,\big|_{f_m} = -\ln(0.5)\,\mathrm{d}V/\mathrm{d}f\,\big|_{f_m} = -\ln(0.5)\mathrm{RBPI}\,\big|_{f_m} \tag{7}$$

This shows that the recession hydrograph from a hydraulic continuum characterized by a quasi-steady-state system is accurately reduced to a simple solution of the differential Eq. (6). As a result, various properties with high diversities and heterogeneities in a runoff system converge on a simple characteristic runoff recession (Sivapalan, 2003; Vaché and McDonnell, 2006).

Hence the RBP given from Tani's (2008) analysis for a sloping permeable domain is clearly linked to the characteristics of a hydraulic continuum as a quasi-steady-state system producing stormflow responses observed in catchments such as CB1 and TEF, although this was only a theoretical consideration for homogeneous conditions. On the basis of this previous analysis, a similarity framework is constructed here to assess the dependencies of RBPI on the dimensionless parameters describing topographic and soil properties.

HESSD
10, 7045–7089, 2013

3.3 Fundamental equations

Like Tani (2008), we also tried to assess a sloping permeable domain with a constant depth and homogeneous hydraulic properties using a two-dimensional form of the Richards equation. A similarity framework was provided by dimensionless forms of the parameters. The origin was placed at the upslope end of the surface of the domain, and the x-axis and z-axis were positive in the horizontal and downward directions, respectively (Fig. 6). For our calculation, we chose the upslope portion of a semi-infinite domain with horizontal length L and vertical depth D in order to avoid the local influences of specific boundary conditions such as seepage faces. Because only a steady state in response to rainfall with a constant intensity is analysed here, the runoff rate in a unit horizontal domain length is also represented by the same value of rainfall intensity. The fundamental equation is given as

$$\frac{\partial}{\partial x}\left(K\frac{\partial \psi}{\partial x}\right)+\frac{\partial}{\partial z}\left\{K\left(\frac{\partial \psi}{\partial z}-1\right)\right\}=0 \tag{8}$$

where K is the hydraulic conductivity and ψ is the pressure head.

As the surface boundary condition, rainfall with a constant intensity f_m was applied to the sloping domain. The infiltration-excess overland flow was eliminated by setting f_m lower than the saturated hydraulic conductivity. The boundary condition along the slope surface was written as

$$q_z = f \ \text{ when } \ \psi < 0 \ \text{ at } \ z = x\tan\omega,\ x \geq 0 \tag{9}$$

where ω is the slope angle. When ψ reached zero, a constant pressure condition ($\psi = 0$) was imposed to calculate the saturation-excess overland flow. As for the other boundary conditions, we assumed that no water flow occurred along the bottom of the permeable domain or across the upslope end. Accordingly,

$$q_z = 0 \ \text{ at } \ z = x\tan\omega + D,\ x \geq 0 \tag{10}$$

HESSD
10, 7045–7089, 2013

$$q_x = 0 \text{ at } x = 0,\ 0 \le z \le D \tag{11}$$

Tani (2008) proposed an approximation for the steady-state distribution of the pressure head based on the Dupuit-Forchheimer assumption (Beven, 1981) and confirmed its agreement with solutions by the Richards equation for a steep-sloping permeable domain. Therefore, we also use this approximation.

For soil physical properties controlling water retention and permeability, Kosugi's (1996, 1997a, b) equations derived from log-normal soil pore distributions,

$$\theta = (\theta_s - \theta_r)S_e + \theta_r = (\theta_s - \theta_r)Q\left[\frac{\ln(\psi/\psi_m)}{\sigma}\right] + \theta_r \text{ for } \psi < 0 \tag{12}$$

$$\theta = \theta_s \text{ for } \psi \ge 0 \tag{13}$$

$$K_0 = K_s K_* \tag{14}$$

were used. Here θ is the volumetric water content, S_e is the effective saturation, θ_s and θ_r are the saturated and residual volumetric water contents, respectively, ψ_m is the median pressure head corresponding to the median pore radius, σ is the standard deviation of the log-transformed soil pore radius ($\sigma > 0$), which characterizes the width of the pore-size distribution, Q is the complementary normal distribution function,

$$Q(y) = (2\pi)^{-0.5}\int_y^\infty \exp\left(\frac{-u^2}{2}\right)\mathrm{d}u \tag{15}$$

HESSD
10, 7045–7089, 2013

K_0 is the hydraulic conductivity given by Kosugi's equation, which is distinguished from K due to the involvement of the macropore effect described later, and K_* is the relative unsaturated hydraulic conductivity, defined as

$$K_* = \left[Q\left\{\frac{\ln(\psi/\psi_m)}{\sigma}\right\}\right]^{1/2} \times \left[Q\left\{\frac{\ln(\psi/\psi_m)}{\sigma} + \sigma\right\}\right]^2 \quad \text{for} \quad \psi < 0 \tag{16}$$

$$K_* = 1 \quad \text{for} \quad \psi \geq 0 \tag{17}$$

Therefore, both the relationships of volumetric water content and unsaturated hydraulic conductivity to pressure head expressed in Eqs. (12), (13), (16), and (17) were represented by parameters including θ_s, θ_r, K_s, ψ_m, and σ. This means that the effects of soil physical properties on the hydraulics of a sloping permeable domain can be assessed by a sensitivity analysis of these five parameters. However, this procedure may be still too tangled to extract the essence of each effect, making a simpler parameter set desirable. First, θ_s and θ_r can be removed using the effective saturation, S_e, because of their linear contribution, and the retention and hydraulic properties can be written in terms of K_s, ψ_m, and σ. In addition, because the saturated hydraulic conductivity K_s may be dependent on the soil pore distribution, K_s and ψ_m can be connected. Kosugi (1997a) proposed the following functional relationship based on the proportional relationship of K_s to the square of the arithmetic mean of pore radius r_a.

$$K_s = Ar_a^2 = Ar_m^2 \exp(\sigma^2) \tag{18}$$

Here r_m is the median pore radius, and A is a proportional constant. The relationship of capillary rise to the pore radius is expressed as

$$\psi = -\frac{2\gamma \cos\eta}{\rho g r} \tag{19}$$

HESSD
10, 7045–7089, 2013

where γ is the surface tension between the water and air, η is the contact angle, ρ is the density of water, and g is the acceleration due to gravity. Substituting Eq. (19) into Eq. (18) yields

$$K_s = A\left[\frac{2\gamma\cos\eta}{\rho g}\right]^2 \frac{1}{\psi_a^2} = \frac{B}{\psi_a^2} = \frac{B\exp(\sigma^2)}{\psi_m^2} \tag{20}$$

where ψ_a is the pressure head corresponding to r_a. Kosugi (1997b) estimated the value of $B[= A\{(2\gamma\cos\eta)/(\rho g)\}^2]$ as $10^{0.4}$ cm^3 s^{-1} from a dataset of soil hydraulic properties (Mashimo, 1960). As the parameter representing soil-water retention, it is better to select ψ_a than ψ_m because K_s is not related to σ, only ψ_a. Hence, the soil physical properties can be represented by only two parameters.

As macropores play an important role in the hydraulics in our permeable domain, their effect was parameterized here by a method proposed by Tani (2008).

$$K = K_0 \quad \text{for} \quad \psi < 0 \tag{21}$$

$$K = \varepsilon \times K_s \quad \text{for} \quad \psi \geq 0 \tag{22}$$

This means that the effect functions only within the saturated zone.

3.4 Categorization of pressure-head distribution in a steady state

From a hydraulic point of view, Tani (2008) categorized the spatial distribution of a pressure-head value in a sloping permeable domain in a steady state into the following three zones, as shown in Fig. 6: the I zone with vertical unsaturated flow, the U zone with unsaturated downslope flow, and the S zone with saturated downslope flow. Regardless of the complex appearance of saturated-unsaturated flow, the pressure-head distribution is simply characterized by this hydraulic zoning. It is therefore useful to

HESSD
10, 7045–7089, 2013

understand the dependence of RBPI on the slope properties. Tani (2008) also formulated indicators partitioning the three zones by the domain depth D, the slope angle ω, the saturated hydraulic conductivity K_s, the standard deviation of the log-transformed soil pore radius σ, and the steady-state flow rate in a unit horizontal domain length f_m equal to the rainfall intensity. The indicators modified into dimensionless form will be described in the following section.

3.5 Similarity framework for a sensitivity analysis

A similarity analysis was sometimes applied to runoff processes to generalize the assessment on the effects of catchment properties on the rainfall-runoff responses (Takagi and Matsubayashi, 1979; Harman and Sivapalan, 2009). Here we introduce a similarity framework to assess the dependence of RBPI on the domain properties, which consist of the slope topography and soil physics. Because RBPI is defined by the increase in V in response to a small increase from a given runoff rate around the average f_m in Eq. (5), f_m was selected as the standard for our dimensionless form. The saturated hydraulic conductivity K_s was made dimensionless as

$$\kappa = \frac{K_s}{f_m} \tag{23}$$

The dimensionless ratio between the depth of the permeable domain and a parameter with the dimension of length representing the soil-water retention curve has often been used for similarity analyses of saturated-unsaturated flow (Verma and Brutsaert, 1970; Tani, 1982, 1985; Suzuki, 1984) because this ratio is a key controller of the relative importance of capillaries with the vertical dimension of the permeable domain (Brutsaert, 2005). Because f_m is used for the standard in our analysis, the parameter l was selected for the length scale in reference to the relationship between K_s and ψ_a in Eq. (20):

$$l = \sqrt{B/f_m} \tag{24}$$

HESSD
10, 7045–7089, 2013

The parameter ψ_a in Eq. (20) is made dimensionless by substituting Eqs. (23) and (24) into Eq. (20), yielding

$$\psi_{a*} = \psi_a / l = -\sqrt{1/\kappa} \tag{25}$$

The soil physical properties are represented by only two dimensionless parameters, κ and σ.

The rainfall intensity f, pressure head ψ, horizontal axis x, vertical axis z, horizontal domain length L, and depth D of the permeable domain are made dimensionless as

$$f_* = f / f_m \tag{26}$$

$$\psi_* = \psi / l \tag{27}$$

$$x_* = x / l \tag{28}$$

$$z_* = z / l \tag{29}$$

$$\lambda = L / l \tag{30}$$

$$\delta = D / l \tag{31}$$

Indicators of the pressure-head distribution in a steady state mentioned in Sect. 3.4 and illustrated in Fig. 6 were made dimensionless as follow: the I zone starts at $x = 0$ but ends at $x = x_{iu}$, after which the U zone grows due to increases in downslope flow. The S zone starts at x_{us}, where the downslope-flow rate within the U zone reaches the maximum limitation. Saturation-excess overland flow starts at x_{so} because of the

HESSD
10, 7045–7089, 2013

maximum in the downslope-flow rate within the S zone. The dimensionless forms of these indicators are

$$x_{\mathrm{iu}*} = \int_{\psi_{f*}}^{\psi_{f*}+\delta\cos^2\omega} K_* d\psi_* \, \kappa \tan\omega \quad \text{for} \quad \alpha < 1 \tag{32}$$

$$x_{\mathrm{iu}*} = \left\{ \int_{\psi_{f*}}^{0} K_* d\psi_* + \varepsilon(\delta\cos^2\omega + \psi_{f*}) \right\} \kappa \tan\omega \quad \text{for} \quad \alpha \geq 1 \tag{33}$$

$$x_{\mathrm{us}*} = \int_{-\delta\cos^2\omega}^{0} K_* d\psi_* \kappa \tan\omega \quad \text{for} \quad \alpha < 1 \tag{34}$$

$$x_{\mathrm{us}*} = \int_{\psi_{f*}}^{0} K_* d\psi_* \kappa \tan\omega \quad \text{for} \quad \alpha \geq 1 \tag{35}$$

$$x_{\mathrm{so}*} = \delta\varepsilon\kappa \sin\omega\cos\omega \tag{36}$$

where the relative hydraulic conductivity K_* for a constant pressure head in the I zone, ψ_{f*}, and dimensionless number α are respectively defined by dimensionless parameters using Eqs. (9), (16), (20), (27), and (31) as

$$K_* = \left[Q\left\{ \frac{\ln(-\psi_*\sqrt{\kappa})}{\sigma} - \frac{\sigma}{2} \right\} \right]^{1/2} \times \left[Q\left\{ \frac{\ln(-\psi_*\sqrt{\kappa})}{\sigma} + \frac{\sigma}{2} \right\} \right]^2 \tag{37}$$

$$K_*(\psi_{f*}) = 1/\kappa \tag{38}$$

HESSD
10, 7045–7089, 2013

$$\alpha = -\frac{\delta \cos^2 \omega}{\psi_{f*}} \tag{39}$$

The spatial distribution of the pressure head ψ_* in the sloping permeable domain in a steady state can be obtained from the flow rate in each zone. ψ_* in the I zone has a constant value, giving a vertical flow rate of

$$\psi_* = \psi_{f*} \tag{40}$$

In the U and S zones, a hydrostatic distribution based on the Dupuit-Forchheimer assumption is applied for a vertical profile as

$$\psi_* = \psi_{b*} - (\delta - z_*)\cos^2 \omega - x_* \sin \omega \cos \omega \tag{41}$$

where ψ_{b*} is the pressure head at the bottom of the domain. The value of ψ_{b*} is inversely calculated from the downslope flow rate across the vertical domain profile at a horizontal distance of x_*, which is equal to the supplied vertical flow rate (the unity in the dimensionless form reflecting f_m in the dimensional form) from the upslope end because the system is in a steady state. The following equations can be used for the calculation based on the categorization of the pressure-head distribution described in Eqs. (32) to (36):

$$\int_{\psi_{f*}}^{\psi_{b*}} K_* d\psi_* = \frac{x_*}{\kappa \tan \omega} \quad \text{for} \quad x_* \le x_{iu*} \quad \text{and} \quad \alpha < 1, \text{or} x_* \le x_{us*} \quad \text{and} \quad \alpha \ge 1 \tag{42}$$

$$\int_{\psi_{b*} - \delta \cos^2 \omega}^{\psi_{b*}} K_* d\psi_* = \frac{x_*}{\kappa \tan \omega} \quad \text{for} \quad x_{iu*} < x_* \le x_{us*} \quad \text{and} \quad \alpha < 1 \tag{43}$$

HESSD
10, 7045–7089, 2013

$$\int_{\psi_{f*}}^{0} K_* d\psi_* + \varepsilon\psi_{b*} = \frac{x_*}{\kappa \tan\omega} \quad \text{for} \quad x_{us*} < x_* \le x_{iu*} \quad \text{and} \quad \alpha \ge 1 \tag{44}$$

$$\int_{\psi_{b*}-\delta\cos^2\omega}^{0} K_* d\psi_* + \varepsilon\psi_{b*} = \frac{x_*}{\kappa \tan\omega} \quad \text{for} \quad x_{us*} < x_* \le x_{so*} \quad \text{and} \quad \alpha < 1,$$

$$\text{or} \quad x_{iu*} < x_* \le x_{so*} \quad \text{and} \quad \alpha \ge 1 \tag{45}$$

3.6 Index of runoff buffering potential (RBPI)

To assess the RBPI, the water storage volume per unit drainage area V is defined as the total volumetric water content θ per unit of horizontal domain length integrated over the whole sloping permeable domain

$$V = \frac{1}{L}\int_0^L \int_{x\tan\omega}^{x\tan\omega+D} \theta \, dz \, dx \tag{46}$$

For our non-dimensionalization described in the last section, the dimensionless storage volume V_* is obtained as

$$V_* = \frac{V - D\theta_r}{I(\theta_s - \theta_r)} = \frac{\int_0^{\lambda}\int_{x_*\tan\omega}^{x_*\tan\omega+\delta} S_e \, dz_* dx_*}{\lambda} \tag{47}$$

The RBPI for f_m in Eq. (5) is made dimensionless into RBPI_* as

$$\mathrm{RBPI}_* \equiv \frac{dV_*}{df_*} = \frac{1}{T_f}\frac{dV}{df}\Big|_{f_m} = \frac{1}{T_f}\mathrm{RBPI}\Big|_{f_m} \tag{48}$$

HESSD
10, 7045–7089, 2013

where T_f is the time scale for the nondimensionalization derived from submitting Eqs. (26), and (47) into (48)

$$T_f = \frac{I(\theta_s - \theta_r)}{f_m} \tag{49}$$

This scale is the time necessary for filling the effective pores in a standard soil depth of I with a standard flow rate of f_m. These theoretical considerations can provide the following advantage for assessing rainfall-runoff responses in a sloping permeable domain. When transient rainfall with an average of f_m is applied to a sloping permeable domain in which a hydraulic continuum is created due to a large supply of rainfall, we can evaluate the effects of the domain properties on the flow rate response as the sensitivity of $RBPI_*$ to five dimensionless parameters: ω, δ, λ, σ, κ, and ε. This advantage can be described for practical use as follows: when it is assumed that there are some hillslopes with various properties and that their soil layers have become wet enough, the effects of these properties on the hydrograph steepness and peak height can be universally assessed by a comparison of the $RBPI_*$ values.

3.7 Recession limbs of the hydrograph

The similarity framework described above using dimensionless parameters is applicable to a dynamic equilibrium with both fluctuations in rainfall intensity and flow rate around the same average value of f_m. As already described in Sect. 2.3, however, this was only a portion of the characteristics of a quasi-steady-state system. The other characteristics emerge in the recession stage of a flow. As the standard parameter of nondimensionalization, f_m may not be suitable because of the transitional change in the recession stage. The soil layer depth D was therefore used instead. The dimensionless variables are defined instead of Eqs. (27) to (30) and (47) as

$$\psi' = \psi / D \tag{50}$$

HESSD
10, 7045–7089, 2013

$$x' = x/D \tag{51}$$

$$z' = z/D \tag{52}$$

$$\lambda' = L/D \tag{53}$$

$$V' = \frac{V - D\theta_r}{D(\theta_s - \theta_r)} \tag{54}$$

The standard flow rate v can be calculated instead of f_m by replacing I with D in Eq. (24), yielding

$$v = B/D^2. \tag{55}$$

Hence

$$f' = f/v \tag{56}$$

Eq. (48) is modified to

$$\mathrm{RBPI}' \equiv \frac{\mathrm{d}V'}{\mathrm{d}f'} = \frac{1}{T_D}\mathrm{RBPI} \tag{57}$$

where T_D, not T_f, is the timescale, with

$$T_D = \frac{D^3(\theta_s - \theta_r)}{B} = \frac{D(\theta_s - \theta_r)}{v} \tag{58}$$

HESSD
10, 7045–7089, 2013

This is the time necessary for filling the effective pores in a standard soil depth of D with the standard flow rate of v. The recession of the flow rate represented by Eq. (6) can be made dimensionless as

$$\frac{\mathrm{d}f'}{\mathrm{d}t'} = \frac{-f'}{\mathrm{d}V'/\mathrm{d}f'} = \frac{-f'}{\mathrm{RBPI}'} \tag{59}$$

The solution of this differential equation is illustrated by a curve with half-life T_h' at f', described as

$$T_\mathrm{h}' = -\ln(0.5)\,\mathrm{d}V'/\mathrm{d}f' = -\ln(0.5)\mathrm{RBPI}' \tag{60}$$

4 Results of the sensitivity analysis

4.1 Sensitivity analysis for RBPI

Figure 7 shows the sensitivity of RBPI_* to κ and λ when $\omega = 30^\circ$, $\delta = 1$, and $\sigma = 1.4$. The left panel is for $\varepsilon = 1$ without any effects of macropores, and the right is for $\varepsilon = 100$ with a large effect. The horizontal distances of indicators categorizing the pressure-head distribution, such as $x_{\mathrm{iu}*}$, $x_{\mathrm{us}*}$, and $x_{\mathrm{so}*}$ in Eqs. (32) to (36), are also plotted along the ordinate axis for the horizontal domain length L. This categorization shows which of the I, U, and S zones compose the vertical profile at any horizontal point along the sloping permeable domain. For example, there is no S zone in the vertical profile of a plot whose ordinate value is smaller than $x_{\mathrm{us}*}$, the I zone exists in plots smaller than $x_{\mathrm{iu}*}$, and saturation-excess overland flow is generated in plots larger than $x_{\mathrm{so}*}$.

In the left panel, high RBPI_* values correspond to high $x_{\mathrm{us}*}$ and $x_{\mathrm{so}*}$ values. This means that RBPI_* has a maximum value when the groundwater table is rising (the I zone is growing), but it rapidly decreases towards the left-upper area ($> x_{\mathrm{so}*}$) because of the saturation-excess overland flow. Along the ridge of RBPI_*, its value decreases with κ because of the effect of the soil physical properties: the volumetric water content in the unsaturated zone of a clayey soil with a small $\kappa (= K_\mathrm{s}/f_\mathrm{m})$ value is close to

HESSD
10, 7045–7089, 2013

saturation, and the increase in the total water storage V in response to a groundwater table rise is small, resulting in a small increase in RBPI_* ($= \mathrm{d}V_*/\mathrm{d}f_*$) compared to that in a sandy soil with a smaller water content in its unsaturated zone. In the right-lower area ($< x_{\mathrm{iU}*}$), RBPI_* is lower for a shorter domain with a higher permeability, indicating its reduction due to rapid drainage there.

In the right panel with a large macropore effect, RBPI_* is generally lower than that in the left panel. This is because of the high drainage capacity of the S zone due to the effect of macropores. An important characteristic is the lack of dependency of RBPI_* on the horizontal domain length λ. Because both the S and U zones are located near the bottom of the domain, the water moves vertically within the I zone, covering most of the domain. Therefore, RBPI_* is almost independent of the horizontal domain length. Only the vertical movement may influence it. For all λ ranges in the right panel and for a small λ range in the left panel, RBPI* becomes smaller toward both large and small ranges of κ. This indicates that RBPI_* only follows $\mathrm{d}S_\mathrm{e}/\mathrm{d}K_*$ in the I zone in a domain with a negligible downslope flow effect in the U and S zones.

4.2 Recession of the flow rate

Figure 8 compares the recession flow rate from $f' = 2.212$ at $t' = 0$. This dimensionless value coincides with $20\,\mathrm{mm\,h^{-1}}$ for the standard length D of 1 m. The time scale T_D is converted to 11.059 h when $\theta_\mathrm{s} - \theta_\mathrm{r}$ is assumed to be 0.1. The upper abscissa axis and right ordinate axis are scaled with these dimensional variables, f and t, whereas the lower and left axes are with the dimensionless variables. The values of the other common parameters of ω and σ were 30° and 1.4, respectively. We used a parameter set of $\lambda' = 20$ and 100 with $\varepsilon = 1$ and 100 for our recession-rate comparison. In addition to the calculation results, the simulation results using Eqs. (1) and (2) with parameters $p = 0.3$ and $k = 25$ that were optimized for a storm event in catchment KT at TEF, as shown in Figs. 3 and 4, are also plotted for the dimensional scale.

For the calculations with no macropore effect ($\varepsilon = 1$), the saturation-excess overland flow was generated when the runoff rate exceeded the threshold indicated by the "×"

HESSD
10, 7045–7089, 2013

mark. This caused a rapid recession, and the weight of the overland flow increased with the horizontal length of the sloping domain. In contrast, a high drainage capacity due to the macropore effect ($\varepsilon = 100$) reduced the rise in the water table and limited the occurrences of overland flow. When the macropore effect is large, the recession of the flow rate depends little on the downslope flow in the U and S zones, but instead is mainly controlled by the vertical water movement in the I zone. The recession flow rates with the macropore effect are consistent with that for KT in Fig. 8, suggesting that the delay in pressure propagation through the vertical water movement had a large possibility of producing the stormflow recession properties observed in small mountainous catchments.

5 Discussion

5.1 Remaining questions regarding stormflow responses

The observations in CB1 and TEF described in Sect. 2 suggest that the stormflow responses could be represented by pressure propagation caused by a hydraulic continuum established due to a large supply of rainfall. The hydraulic continuum is theoretically characterized by a quasi-steady-state system conceptualized by a tank with a drainage hole, where the increase/decrease speed of the flow rate $\mathrm{d}f/\mathrm{d}t$ from the continuum depends upon RBPI, the differential coefficient of storage with respect to the flow rate in a steady state $\mathrm{d}V/\mathrm{d}f$. Therefore, RBPI controls the delay in the flow response, making the flow peak lower and the recession limb gentler. The similarity analysis in Sect. 3 provided a methodology with which to quantify the sensitivity of RBPI to the topographical and soil properties of sloping permeable domains. The macropore effect supported the small range of RBPI (Fig. 7) and decreased the effect of the downslope flow (Fig. 8). Nevertheless, it is still an open question as to why macropores generally develop, even though their role in the stormflow response is well understood.

HESSD
10, 7045–7089, 2013

The reason may be a long time-scale evolution process involving tectonic activity, as discussed below.

5.2 Effects of soil-layer evolution

In a region with high tectonic activity and frequent heavy storms such as Japan, topographic evolution on a timescale of over 10^5 yr accompanied by strong erosional force produces steep mountainous terrain (Montgomery and Brandon, 2002). A zero-order catchment is created through the topographic evolution processes (Tsukamoto, 1973), and landslides more frequently occur in hollows with concave topography than in other areas of a catchment because of water convergence (Tsukamoto et al., 1982). However, analyses of cosmogenic nuclides demonstrated that soil is constantly denuded even along the ridge lines surrounding hollows in zero-order catchments (Heimsath, 1999), at speeds of about 0.1–1.0 mm yr^{-1} in Japan (Matsushi and Matsuzaki, 2010). These studies suggest that soil produced from weathered bedrock continually moves from a ridge down to a concave hollow by gravity, though there is not yet enough detailed field evidence to validate this mechanism. Soil creep and small landslides may also contribute to this erosion process from the ridge line to the hollow. Hence we can estimate a dynamic cycle of soil evolution processes, including landslides, on timescales of 10^2 to 10^4 yr in a zero-order catchment created by topographic evolution on a longer timescale. Soil-layer evolution may start after a landslide only when soil particles on a denuded bedrock surface overcome the strong erosion forces from tectonic activity and heavy storms (Iida, 1999).

Two kinds of preconditions are absolutely necessary for soil-layer evolution: soil particles produced from the denuded surface of weathered bedrock are so easily eroded by heavy rainfall that support by vegetation roots plays a key role in the soil evolution (Shimokawa, 1984). When a denuded area is created by a landslide, vegetation and soil recover from the edge of the area through seeds supplied along with soil particles from surrounding areas (Matsumoto et al., 1995). Observations of bare land located in a granite mountain in Japan (Fukushima, 2006) suggested that in a widespread

HESSD
10, 7045–7089, 2013

denuded landscape, the soil cannot be semi-eternally recovered. This is because the cooperation between vegetation and soil fails owing to a poor seed supply. The effect of vegetation roots on slope stability is quite important even for a thick soil layer because of the effects of both root penetration perpendicular to the sliding surface and three-dimensional root entanglement (Kitahara, 2010).

In addition to the vegetation effect, the drainage capacity of water is also important in soil layer evolution. According to studies of hillslope stability, the safety factor of a soil layer decreases as the groundwater table rises (e.g., Sidle et al., 1985). When overland flow is generated by water saturation, even a gentle slope may fail and result in debris flows (Takahashi, 1978). If a landslide does not occur during a storm event within a zero-order catchment, we can infer that the slope might have remained stable across the entire area. This suggests that an efficient drainage system consisting of macropores and/or natural pipes may assist reductions in the groundwater rise, at least in steep hollows where water converges. Because this assistance is efficient throughout the period of soil-layer evolution, it would be accompanied by the development of the drainage system. Erosion of fine soil particles along the groundwater flow contributes to the development of a drainage system, which can inhibit the reduction of the safety factor in response to an increase of the soil-layer thickness. Thus, we can conclude that the development of efficient drainage systems along a hollow are inevitably associated with the evolution of the soil layer.

5.3 Rapid stormflow responses

From the viewpoint of rainfall-stormflow responses, the simple characteristic described in Sect. 2 is ensured by efficient drainage systems. This characteristic is robust for any storm magnitude, as long as the soil layer is not lost due to landslides. However, the safety factor decreases gradually on long time scales, both through the soil layer evolution and the uplifting of the mountain body by tectonic activity (Montgomery and Brandon, 2002). Therefore, the soil-layer evolution cannot continue forever. The robustness will eventually fail, and once a landslide occurs, a large amount of water stored within

HESSD
10, 7045–7089, 2013

the soil layer will be instantaneously released, causing fluidization of the collapsed soil (Takahashi, 1978). As a result, stormflow responses from soil layers in a zero-order catchment can provide simple characteristics that can be consistently simulated by a tank with a drainage hole throughout a wide range of storm magnitudes. The rapidity of stormflow responses and their recession limbs is generally derived from the pressure propagation of the hydraulic continuum created in a soil layer as explained in Sect. 2. However, Sect. 4 demonstrated that saturation-excess overland flow generally occurs unless the macropore effect inhibits the groundwater table. In a zero-order catchment, the convergence of water into a hollow increases the opportunity for overland flow, but efficient drainage pathways consisting of macropores and natural pipes inhibit the occurrence of overland flow and contribute to a self-preserving evolution of the soil layer. Therefore, we can conclude that the quickness of stormflow responses in a zero-order catchment is inevitably derived from the soil layer evolution.

5.4 A possible modelling strategy

According to our discussion, the evolution of the soil layer may control complex and heterogeneous spatial distributions of topographic and soil properties, including macropores and natural pipes in a zero-order catchment. However, the evolution may also allow quick stormflow responses with small deviations. Both phenomena are produced from the same process, but it is difficult to find a direct relationship between them because the intervention arises from the long evolutionary history. For example, if more efficient drainage pathways develop in clayey soil than in sandy soil through a long history of soil-layer evolution, the dependency of stormflow responses on the soil physical properties might not be follow the characteristic expected. Therefore, to predict the dependence of the catchment properties on stormflow responses using a distributed runoff model, it is necessary to parameterize the properties considering the historical evolution of the soil layer. Because it is difficult to quantify which property is sensitive to stormflow, a methodology of comparative hydrology may also need to be conducted to detect sensitive properties before our parameterization strategy is applied.

HESSD
10, 7045–7089, 2013

6 Conclusions

The review in Sect. 2 demonstrated that although the allocation of rainfall to the stormflow is controlled by deep infiltration and storage within a low matric potential, the stormflow response reflects pressure propagation from the hydraulic continuum established in the soil layer when enough rainfall is supplied. Section 3 described a similarity analysis for quantifying the sensitivity of the stormflow response and recession limb to the topographic and soil properties, including the macropore effect. Section 4 showed that the deviation of stormflow responses decreases due to the macropore effect. The discussion in Sect. 5 suggested that such quick stormflow responses with small deviations might be derived from the evolution of the soil layer. On the basis of these findings, we have proposed two strategies for stormflow prediction: a parameterization of catchment properties considering the historical evolution of a soil layer, and comparative hydrology for detecting sensitive properties.

Acknowledgements. I express my appreciation to Associate Professor Suzanne Anderson (University of Colorado, Boulder) for providing valuable data on the sprinkler experiment conducted in CB1 with useful comments. Data from TEF were obtained while I worked for the Forestry and Forest Products Research Institute, and I wish to thank all the staff concerned. This study was supported by the Japan Society for the Promotion of Science (JSPS) for KAKENHI Grant Number 23221009, titled "Prediction of catchment runoff changes based on elucidating a nested structure consisting of the developments of topography, soil and vegetation".

References

Anderson, S. P., Dietrich, W. E., Montgomery, D. R., Torres, R., Conrad, M. E., and Loague, K.: Subsurface flow paths in a steep, unchanneled catchment, Water Resour. Res. 33, 2637–2653, 1997.

Betson, R. P. and Ardis Jr., C. V.: Implications for modelling surface-water hydrology, in: Hillslope Hydrology edited by: Kirkby, M. J., Wiley & Sons, Chichester, UK, 295–323, 1978.

Beven, K.: Kinematic downslope flow, Water Resour. Res., 17, 1419–1424, 1981.

HESSD

10, 7045–7089, 2013

Beven, K. and Kirkby, M. J.: A physically based, variable contributing area model of basin hydrology, Hydrolog. Sci. Bull., 24, 43–69, 1979.
Brutsaert, W.: Hydrology: An Introduction, Cambridge Univ., Cambridge, ISBN 13 978-0-521-82479-8, 366–382, 2005.
Dunne, T. and Black, R. D.: Partial-area contributions to storm runoff in a small New England watershed, Water Resour. Res., 6, 1296–1311, 1970.
Ebel, B. R., Loague, K., Dietrich, W. E., Montgomery, D. R., Torres, R., Anderson, S. P., and Giambelluca, T. W.: Near-surface hydrologic response for a steep, unchanneled catchment near Coos Bay, Oregon: 1. Sprinkled experiments, Am. J. Sci., 907, 678–708, doi:10.2475/04.2007.02, 2007.
Freeze R. A.: Role of subsurface flow in generating surface flow 2. Upstream source areas, Water Resour. Res., 8, 1272–1283, 1972.
Fukushima, Y.: The role of forest on the hydrology on headwater wetlands, in: Environmental Role of Wetlands in Headwaters edited by: Krecek, J. and Haigh, M., Springer, Dordrecht, ISBN 1-4020-4226-4, 17–47, 2006.
Fukushima, Y. and Suzuki, M.: A model for river flow forecasting for a small mountain catchment, Hydrol. Process., 2, 167–185, 1988.
Gabrielli, C. P., McDonnell, J. J., and Jarvis, W. T.: The role of bedrock groundwater in rainfall–runoff response at hillslope and catchment scales, J. Hydrol., 450–451, 117–133, doi:10.1016/j.jhydrol.2012.05.023, 2012.
Gomi, T., Asano, Y., Uchida, T., Onda, Y., Sidle, R. C., Miyata, S., Kosugi, K., Mizugaki, S., Fukuyama, T., and Fukushima, T.: Evaluation of storm runoff pathways in steep nested catchments draining a Japanese cypress forest in central Japan: a hydrometric, geochemical, and isotopic approaches. Hydrol. Process., 24, 550–566, doi:10.1002/hyp.7550, 2010.
Harman, C. and Sivapalan, M.: A similarity framework to assess controls on shallow subsurface flow dynamics in hillslopes, Water Resiour. Res., 45, W01417, doi:10.1029/2008WR007067, 2009.
Heimsath, A. M., Dietrich, W. E., Nishiizumi, K., and Finkel, R. C.: Cosmogenic nuclides, topography, and the spatial variation of soil depth, Geomorphology, 27, 151–172, 1999.
Hewlett, J. D. and Hibbert, A. R.: Factors affecting the response of small watersheds to precipitation in humid areas, in: International Symp. Forest Hydrology, edited by: Sopper, W. E. and Lull, H. W., Pergamon, Oxford, 275–290, 1968.

HESSD
10, 7045–7089, 2013

Hewlett, J. D. and Nutter, W. L.: The varying source area of streamflow from upland basins, in: Proc. Symp. Interdisciplinary Aspects of Watershed Management, American Society of Civil Engineers, New York, 65–83, 1970.
Horton, R. E.: The role of infiltration in the hydrologic cycle, T. Am. Geophys. Union, 14, 446–460, 1933.
Hosoda, I.: Measurement on groundwater level variations within the bedrock in a hillslope underlain by Palaeozoic formations, Proceedings of 2008 Annual Conference, Japan Society of Hydrology and Water Resources, 172–173, 2008 (in Japanese).
Iida, T.: A stochastic hydro-geomorphological model for shallow landsliding due to rainstorm, Catena, 34, 293–313, doi:10.1016/S0341-8162(98)00093-9, 1999.
Ishihara, T. and Takasao, T.: A study on the transformation system during flood runoff, Bull. Disasaster Prev. Res. Inst., Kyoto Univ., 7, 265–279, 1964 (in Japanese with English abstract).
Iwagaki, Y.: Fundamental studies on the runoff analysis by characteristics, Disasaster Prev. Res. Inst. Bull., 10, Kyoto Univ., Kyoto, 25 pp., 1955.
Katsuyama, M., Fukushima, K., and Tokuchi, N.: Comparison of rainfall-runoff characteristics in forested catchments underlain by granitic and sedimentary rock with various forest ages, Hydrol. Res. Lett., 2, 14–17, doi:10.3178/HRL.2.14, 2008.
Katsuyama, M., Tani, M., and Nishimoto, S.: Connection between streamwater mean residence time and bedrock groundwater recharge/discharge dynamics in weathered granite catchments, Hydrol. Process., 24, 2287–2299, doi:10.1002/hyp.7741, 2010.
Kimura, T.: The Flood Runoff Analysis Method by the Storage Function Model, The Public Works Research Institute, Ministry of Construction, Tokyo, 1961 (in Japanese).
Kitahara, H.: Effect of tree root systems on slope stability, Suirikagaku, 311, 11–37, 2010 (in Japanese).
Kosugi, K.: Lognormal distribution model for unsaturated soil hydraulic properties, Water Resour. Res., 32, 2697–2703, 1996.
Kosugi, K.: Effect of pore radius distribution of forest soils on vertical water movement in soil profile, J. Japan Soc. Hydrol. Water Resour., 10, 226–237, 1997a.
Kosugi, K.: New diagrams to evaluate soil pore radius distribution and saturated hydraulic conductivity of forest soil, J. For. Res.-Jpn., 2, 95–101, 1997b.
Kosugi, K., Katsura, S., Katsuyama, M., and Mizuyama, T.: Water flow processes in weathered granitic bedrock and their effects on runoff generation in a small headwater catchment, Water Resour. Res. 42, W02414, doi:10.1029/2005WR004275, 2006.

HESSD
10, 7045–7089, 2013

Kosugi, K., Fujimoto, M., Katsura, S., Kato, H., Sando, Y., and Mizuyama, T.: Localized bedrock aquifer distribution explains discharge from a headwater catchment, Water Resour. Res., 47, doi:10.1029/2010WR009884, 2011.
Mashimo, Y.: Studies on the physical properties of forest soil and their relation to the growth of sugi (*Cryptomeria japonica*) and hinoki (*Chamaecyparis obtusa*), Forest Soils of Japan Report 11, Government Forest Experimental Station, Tokyo, 182, 1960 (in Japanese with English abstract).
Matsumoto, M., Shimokawa, E., and Jitousono, T.: A natural recovegetation process on shallow landslide scars in deep weathering granite slopes, Res. Bull. Kagoshima Univ. For., 23, 55–79, 1995 (in Japanese with English abstract).
Matsushi, Y. and Matsuzaki, H.: Denudation rates and threshold slope in a granitic watershed, central Japan. Nucl. Instrum. Meth. B, 268, 1201–1204, 2010.
McDonnell, J. J.: A rationale for old water discharge through macropores in a steep, humid catchment, Water Resour. Res., 26, 2821–2832, 1990.
McDonnell, J. J.: Where does water go when it rains? Moving beyond the variable source area concept of rainfall-runoff response, Hydrol. Process., 17, 1869–1875, 2003.
Meadows, D. H.: Thinking in Systems: A Primer, edited by: Wright, D., Earthscan, London, 218, ISBN 978-1-84407-726-7, 2008.
Montgomery, D. R. and Brandon, M. T.: Topographic controls on erosion rates in tectonically active mountain ranges, Earth Planet. Sc. Lett., 201, 481–489, doi:10.1016/S0012-821X(02)00725-2, 2002.
Montgomery, D. R. and Dietrich, W. E.: Runoff generation in a steep, soil-mantled landscape, Water Resour. Res. 38, 1168, doi:10.1029/2001WR000822, 2002.
Montgomery, D. R., Dietrich, W. E. Torres, R., Anderson, S. P., Heffner, J. T., and Loague, K.: Piezometric response of a steep unchanneled valley to natural and applied rainfall, Water Resour. Res., 33, 91–109, 1997.
Mosley, M. P.: Streamflow generation in a forested watershed, New Zealand, Water Resour. Res., 15, 795–806, 1979.
Okamoto, Y.: The studies on the runoff phenomena and processes of mountain forest drainage basins in Japan, Proc. JSCE, 280, 51–66, 1978 (in Japanese with English abstract).
O'Loughlin, E. M.: Prediction of surface saturation zones in natural catchments by topographic analysis, Water Resour. Res., 22, 794–804, 1986.

HESSD
10, 7045–7089, 2013

Onda, Y., Komatsu, Y., Tsujimura, M., and Fujihara, J.: The role of subsurface runoff through bedrock on storm flow generation, Hydrol. Process., 15, 1693–1706, 2001.
Pearce, A. J., Stewart, M. K., and Sklash, M. G.: Storm runoff generation in humid headwater catchments: 1. Where does the water come from?, Water Resour. Res., 22, 1263–1272, 1986.
Pinder, G. F. and Jones, J. F.: Determination of the ground-water component of peak discharge from the chemistry of total runoff, Water Resour. Res., 5, 438–445, 1969.
Rubin, J. and Steinhardt, R.: Soil water relations during rain infiltration: I. Theory, Soil Sci. Soc. Am. Proc., 27, 246–251, 1963.
Shimizu, T.: Relation between scanty runoff from mountainous watershed and geology, slope and vegetation, B. For. and For. Prod. Res. Inst., 310, 109–128, 1980 (in Japanese with English abstract).
Shimokawa, E.: A natural recovery process of vegetation on landslide scars and landslide periodicity in forested drainage basins, in: Proc. Symp. Effects of Forest Land Use on Erosion and Slope Stability, East-West Center, University of Hawaii, Honolulu: 99–107, 1984.
Sidle, R. C., Pearce, A. J., and O'Loughlin, C. L.: Hillslope Stability and Land Use, Am. Geophys. Union, Washington DC, ISBN 0-87590-315-0, 19–30, 1985.
Sivapalan, M.: Process complexity at hillslope scale, process simplicity at the watershed scale: is there a connection?, Hydrol. Process., 17, 1037–1041, doi:10.1002/hyp.5109, 2003.
Sivapalan, M., Takeuchi, K., Franks, S. W., Gupta, V. K., Karambiri, H., Lakshim, V., Liang, X., McDonnell, J. J., Mendiondo, E. M., O'Connell, P. E., Oki, T., Pomeroy, J. W., Schertzer, D., Uhlenbrook, S., and Zehe, E.: IAHS Decade on predictions in ungauged basins (PUB), 2003–2012: Shaping an exciting future for the hydrological sciences, Hydrolog. Sci. J., 48, 857–880, 2003.
Sklash, M. G. and Farvolden, R. N.: The role of groundwater in storm runoff, J. Hydrol., 43, 45–65, 1979.
Soil Conservation Service: National Engineering Handbook, Section 4 Hydrology, US Department of Agriculture, Washington DC, 1972.
Sueishi, T.: On the runoff- analysis by the method of characteristics – Hydraulic studies on the run-off phenomena of rain water 2nd report, Proc. JSCE, 29, 74–87, 1955 (in Japanese with English abstract).
Sugawara, M.: Runoff Analysis Part 2, Kyoritsu, Tokyo, 56–57, 1979 (in Japanese).

HESSD
10, 7045–7089, 2013

Sugawara, M.: Tank model, in: Computer Models in Watershed Hydrology, edited by: Singh, V. J., Water Resources Publications, Highland Ranch, 165–214, 1995.
Sugawara, M. and Katsuyama, Y.: On runoff mechanisms in Takaragawa Experimental Watersheds, Science and Technology Agency, Tokyo, 69 pp., 1957 (in Japanese).
Sugiyama, H., Kadoya, M., Nagai, A., and Lansey, K.: Evaluation of the storage function model parameter characteristics, J. Hydrol., 191, 332–348, 1997.
Suzuki, M.: The properties of a baseflow recession on small mountainous watersheds (I) Numerical analysis using saturated-unsaturated flow model, J. Jap. For. Soc., 66, 174–182, 1984 (in Japanese with English abstract).
Takagi, F. and Matsubayashi, U.: On the non-linearity of sub-surface and groundwater-runoff, Proc. JSCE, 283, 45–55, 1979 (in Japanese).
Takahashi, T.: Mechanical characteristics of debris flow, J. Hydraul. Div.-ASCE, 1048, 1153–1169, 1978.
Tani, M.: The properties of a water-table rise produced by a one-dimensional, vertical, unsaturated flow, J. Jap. For. Soc., 64, 409–418, 1982 (in Japanese with English abstract).
Tani, M: The effects of soil physical properties on the groundwater-table rise, Proceedings of the Internat. Symp. Erosion, Debris Flow and Disaster Prevention, edited by: Takei, A., The Erosion Control Engineering Society, Japan, Tokyo, 361–365, 1985.
Tani, M.: Runoff generation processes estimated from hydrological observations on a steep forested hillslope with a thin soil layer, J. Hydrol., 200, 84–109, 1997.
Tani, M.: Analysis of runoff-storage relationships to evaluate the runoff-buffering potential of a sloping permeable domain, J. Hydrol., 360, 132–146, doi:10.1016/j.jhydrol.2008.07.023, 2008.
Tani, M. and Abe, T.: Analysis of stormflow and its source area expansion through a simple kinematic wave equation, Forest Hydrology and Watershed Management, IAHS Publ., 167, 609–615, 1987.
Tani, M. and Hosoda, I.: Dependence of annual evapotranspiration on a long natural growth of forest and vegetation changes, J. Japan Soc. Hydrol. Water Resour., 25, 71–88, 2012 (in Japanese with English abstract).
Tani, M., Fujimoto, M., Katsuyama, M., Kojima, N., Hosoda, I., Kosugi, K., Kosugi, Y., and Nakamura, S.: Predicting the dependencies of rainfall-runoff responses on human forest disturbances with soil loss based on the runoff mechanisms in granitic and sedimentary-rock mountains, Hydrol. Process., 26, 809–826, doi:10.1002/hyp.8295, 2012.

HESSD
10, 7045–7089, 2013

Tromp-van Meerveld, H. J. and McDonnell, J. J.: Threshold relations in subsurface stormflow 1. A 147 storm analysis of the Panola hillslope, Water Resour. Res., 42, W02410, doi:10.1029/2004WR003778, 2006.

Tsukamoto, Y.: Study on the growth of stream channel I – relatiosnhip between stream channel rowth and landslides occurring during heavy storm, J. Japan Soc. Erosion Control Engineering, 87, 4–13, 1973 (in Japanese).

Tsukamoto, Y., Ohta, T., and Noguchi, H.: Hydrological and geomorphological studies of debris slides on forested hillslopes in Japan, in: Recent developments in the explanation and prediction of erosion and sediment yield, IAHS Publ., 137, 89–98, 1982.

Vaché, K. B. and McDonnell, J. J.: A process-based rejectionist framework for evaluating catchment runoff model structure, Water Resour. Res., 42, W02409, doi:10.1029/2005WR004247, 2006.

Verma, R. D. and Brutsaert, W.: Unconfined aquifer seepage by capillary flow theory, J. Hydraul. Div.-ASCE, 96HY6, 1331–1344, 1970.

HESSD
10, 7045–7089, 2013

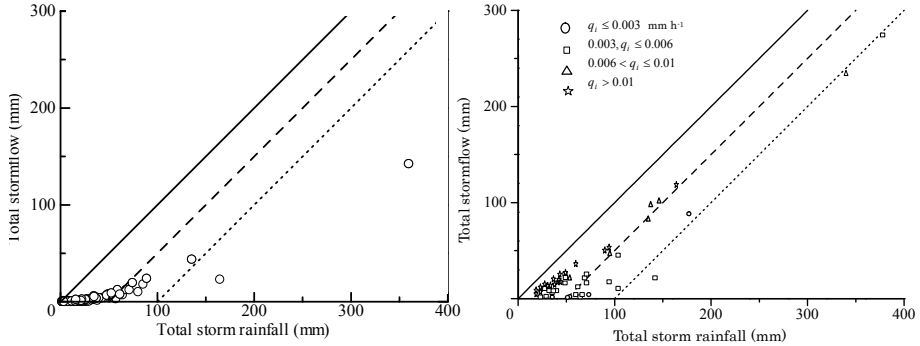

Fig. 1. Relationship between the total stormflow and the total storm-event rainfall. Left: Kiryu, right: KT in TEF. q_i: runoff rate before the storm event. Solid, broken, and dotted lines respectively indicate $Q = R$, $Q = R - 50$, $Q = R - 100$, respectively, where R is the total storm rainfall and Q is the total stormflow. After Katsuyama et al. (2008) for Kiryu and Tani and Abe (1987) for KT.

HESSD
10, 7045–7089, 2013

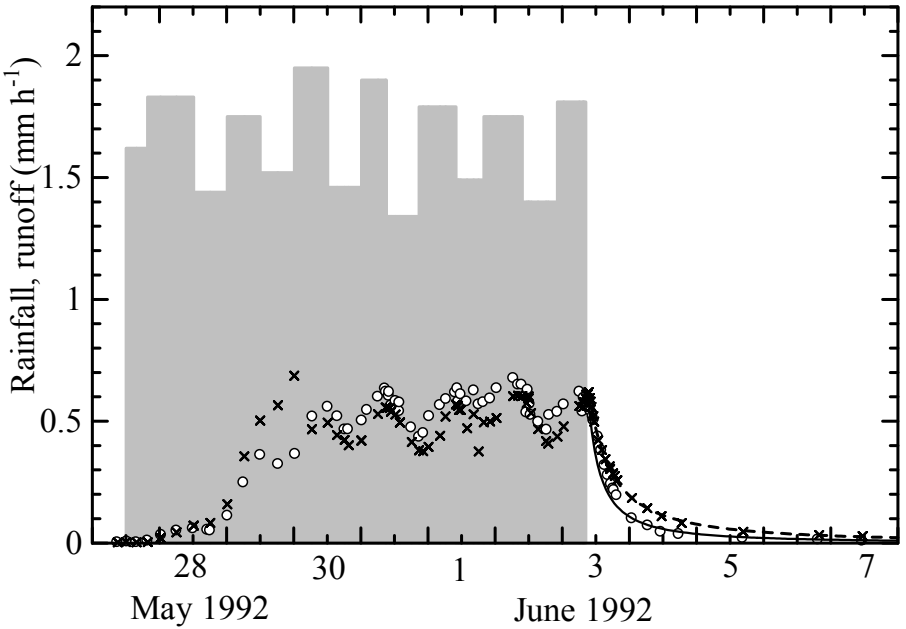

Fig. 2. Sprinkled rainfall and runoff responses in CB1. Bar: rainfall, ∘: runoff rate at the upper weir, ×: runoff rate at the lower weir. The solid and broken lines were calculated for a tank with a drainage hole using the functional relationship between storage and runoff in Eq. (2), with a p value of 0.3 and k values of 11 for the upper weir and 20 for the lower weir. Recreated from Fig. 3 of Anderson et al. (1997); courtesy of Suzanne Anderson.

HESSD
10, 7045–7089, 2013

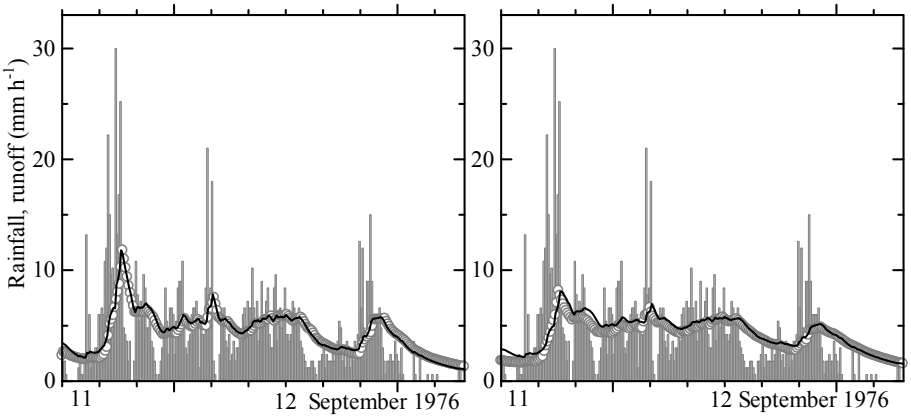

Fig. 3. Storm hydrographs observed and simulated by a tank with a drainage hole in response to a typhoon storm in September 1976 at KT (left) and MN (right) in TEF. Bar: 10 min rainfall intensity (displayed in mm h^{-1}). ∘: observed runoff. Line: simulated runoff rate. The lines were calculated for a tank with a drainage hole using the functional relationship between storage and runoff given by Eq. (2), with a common p value of 0.3 and k values of 25 for KT and 40 for MN.

HESSD
10, 7045–7089, 2013

A paradigm shift in stormflow prediction through pressure propagation analysis

Makoto Tani

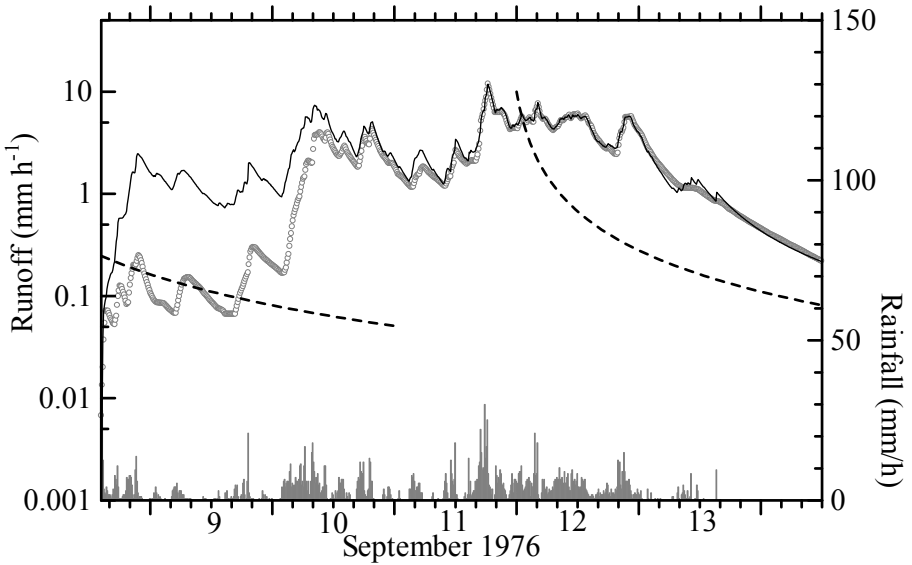

Fig. 4. Same as Fig. 3 but plotted only for KT in a semi-logarithmic runoff scale. ∘: observed. Solid line: calculated. Broken line: long-term recession curve calculated using the same parameter values.

HESSD
10, 7045–7089, 2013

A paradigm shift in stormflow prediction through pressure propagation analysis

Makoto Tani

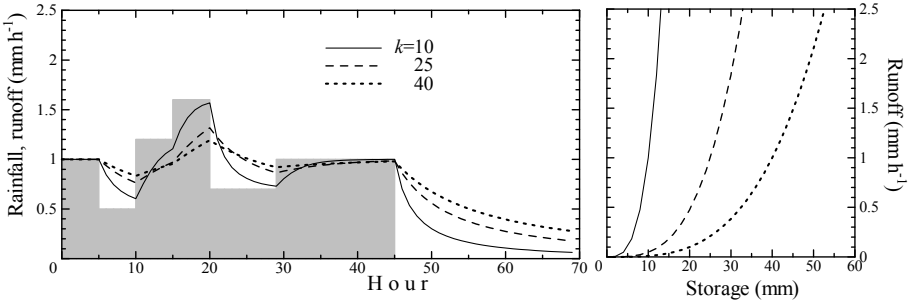

Fig. 5. A schematic example of flow rates calculated for a tank with a drainage hole in response to fluctuations in rainfall around the average rate of 1 mm h^{-1} and their recession limbs after the rainfall stopped. The functional relationships between storage and runoff used in the calculations with a common p value of 0.3 in the left panel are displayed in the right panel.

HESSD
10, 7045–7089, 2013

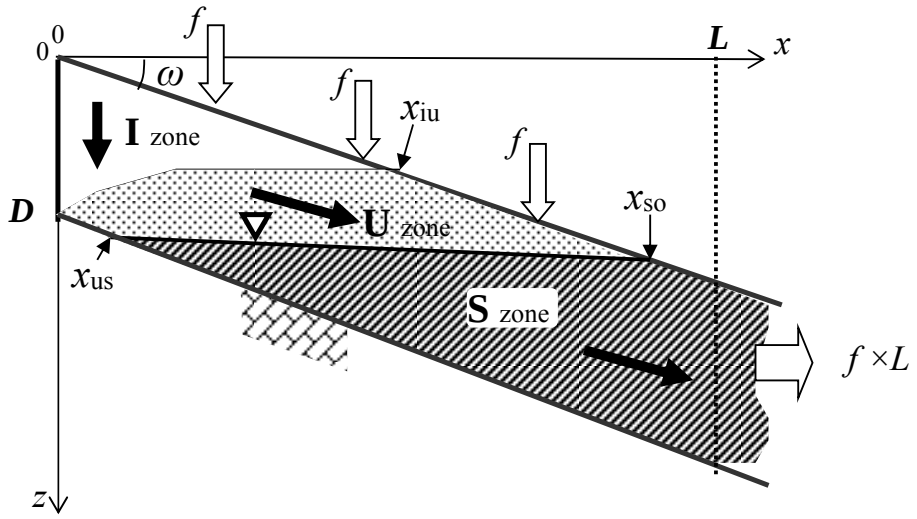

Fig. 6. Schematic of a sloping permeable domain with approximated categorization of the pressure head (I, U, and S zones). The horizontal distances involving the categorization of x_{iu}, x_{us}, and x_{so} are also plotted.

HESSD
10, 7045–7089, 2013

A paradigm shift in stormflow prediction through pressure propagation analysis

Makoto Tani

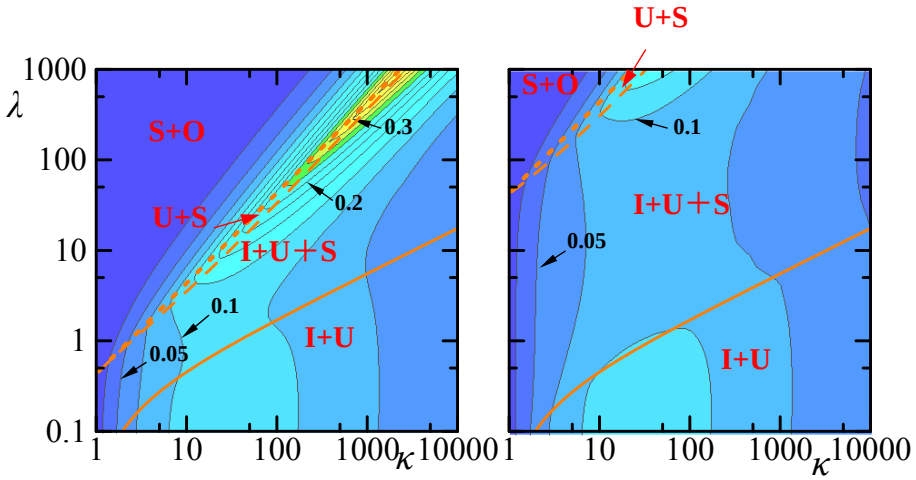

Fig. 7. Contour plots of RBPI* against κ and λ for $\varepsilon = 1$ (left) and 100 (right). Orange solid, dashed, and dotted lines represent the horizontal distances for the end point of the I zone (x^*_{iu}), the start point of the S zone (x^*_{us}), and the start point of the saturation-excess overland flow (x^*_{so}), respectively. The red letters indicate which zones are included in the vertical profile at each horizontal point of the sloping domain (see Fig. 6).

HESSD
10, 7045–7089, 2013

A paradigm shift in stormflow prediction through pressure propagation analysis

Makoto Tani

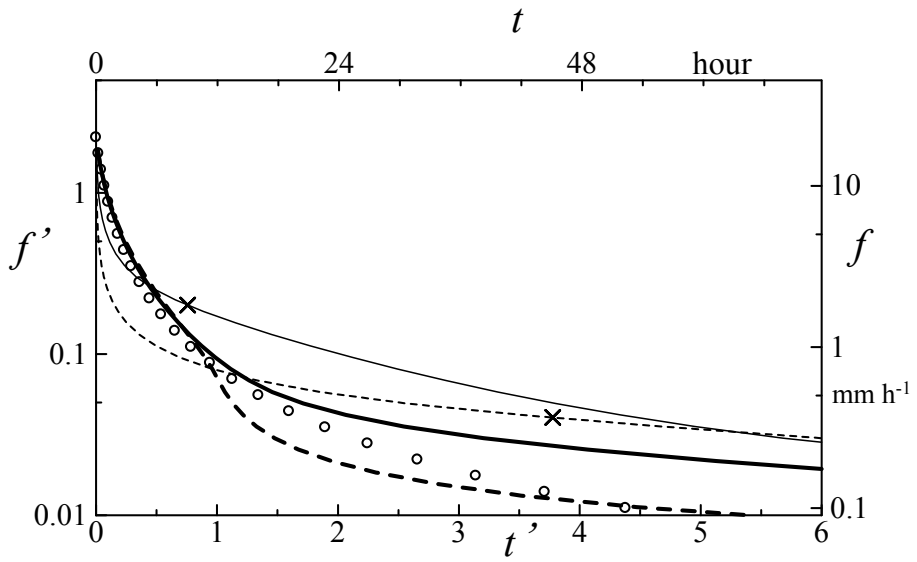

Fig. 8. Runoff recession of the flow rate from a sloping permeable domain Dimensionless scales are used for the bottom and left axes, and dimensional scales converted by $D = 100$ m are used for the top and right axes. Thin solid: $\lambda' = 20$ and $\varepsilon = 1$, thin broken: $\lambda' = 100$ and $\varepsilon = 1$. Thick solid: $\lambda' = 20$ and $\varepsilon = 100$, thick broken: $\lambda' = 100$ and $\varepsilon = 100$. ×: the f' rate in which the saturation-excess overland flow is generated at the downslope end of the domain. ∘: calculated by the storage-runoff relationship optimized for catchment KT, as also shown in Figs. 3 and 4.

HESSD
10, 7045–7089, 2013